THE ASTROPHYSICAL JOURNAL, 415:708–714, 1993 October 1

HIGH SPATIAL RESOLUTION OBSERVATIONS OF CO IN CRL 618

KATSUNORI M. SHIBATA,[1,2] SHUJI DEGUCHI,[1] NAOMI HIRANO,[3] OSAMU KAMEYA,[4] AND SHIN'ICHI TAMURA[5]

Received 1992 August 31; accepted 1993 April 12

ABSTRACT

We have made aperture synthesis observations of the very young planetary nebula CRL 618 by ^{12}CO $J = 1$–0 line and continuum at 115.271 GHz with the Nobeyama Millimeter Array. The maps with the angular resolution of 3".6 × 3".5 show strong concentration of CO toward the ionized core with no clear evidence of a toroidal structure around the star nor along the axis of visible bipolar lobes. Velocity-channel maps show complex structures characterized by a spheroidal component weakly elongated to the east-west direction and a hornlike feature which looks to be spread from the center in a narrow opening angle. It seems difficult to interpret the maps by the simple model with a smooth outflow. The disk structure does not show up in our observation because of the smallness of the disk or obscuring by the surrounding thick spherical CO gas. We detected the red wing component of a high-velocity outflow but not the blue wing component. The red wing arises from the compact region, within 2" from the ionized core, and suggests that the high-velocity outflow occurs in a compact region centered on the ionized core. The 115 GHz continuum emission has been detected with the total flux density of 1.48 Jy and it is a point source centered on the ionized core.

Subject headings: ISM: kinematics and dynamics — planetary nebulae: individual (CRL 618) — radio lines: ISM

1. INTRODUCTION

Asymptotic giant branch (AGB) stars with intermediate initial mass (1 to 5–8 $M_\odot$) begin a transition to the planetary nebula nucleus when their envelope masses reduce to about 10^{-3} $M_\odot$. The ejected matters, surrounding its progenitor star, are swept up by fast wind from the central star and become to be seen as planetary nebula due to ionization by UV radiation from the central star. Hence, the circumstellar envelope ejected at the AGB stage contains the history of past mass loss and also affects the formation and shaping process of planetary nebula.

The infrared source CRL 618 is an important object for the investigation of the formation and evolution of planetary nebulae. It is at the transition stage to the planetary nebulae. It has a carbon-rich envelope and shows strong, rich molecular lines such as CO, CS, HCN, HCO^+, HC_3N and H_2CO, etc., (Bachiller et al. 1988; Bujarrabal et al. 1988; Cernicharo et al. 1989; Deguchi, Claussen, & Goldsmith 1986; Gammie et al. 1989). In optical wavelength, it shows bipolar lobes of about 3" in diameter separated by 7" along the east-west direction, and shows a strong infrared peak at the midpoint of the lobes (Westbrook et al. 1975). From the optical measurement of linear polarization (Schmidt & Cohen 1981) it is deduced that the bulk of permitted lines from the lobes are formed in a central ionized gas and are scattered by dust grains in the lobes, and forbidden lines and the rest of permitted lines are formed in a weakly ionized gas within the lobes. Carsenty & Solf (1982) examined the kinematical structure of ionized gas using a high-dispersion spectrograph and suggested that the polar axis of optical bipolar lobes inclines by 45° with respect to the plane of the sky and that the ionized gas expand with the velocity of 80 km s^{-1} along the axis. The observations of H_2 $v = 1$–0 S(1) 2.12 μm emission have made by Thronson (1981), Beckwith, Beck, & Gatley (1984) and Burton & Geballe (1986). They suggested from the distribution and the profile of H_2 $v = 1$–0 S(1) 2.12 μm emission were made by Thronson region produced in the visible lobes by a fast wind from the central star. Wynn-Williams (1977) had detected radio continuum emission from CRL 618 and Kwok & Feldman (1981) showed that the continuum flux density at the wavelength of 6, 3, and 2 cm had increased by a factor of 2 between 1977 and 1980. Kwok & Bignell (1984) made radio continuum maps by VLA and found a very compact radio core of the size 0".4 × 0".1.

Maps by ^{12}CO $J = 1$–0, $J = 2$–1 and HC_3N $J = 17$–16 lines were made with the IRAM 30 m telescope (Bachiller et al. 1988; Bujarrabal et al. 1988) and showed that deconvolved sizes at half intensity were about 20", 11", and 10" by the CO $J = 1$–0, $J = 2$–1, and HC_3N maps, respectively. Bachiller et al. (1988) determined a mass-loss rate of 10^{-4} $M_\odot$ yr^{-1} from the CO profile. Recently, a high-velocity outflow with a terminal velocity of about 200 km s^{-1} was detected in CO, HCN, HC_3N and HCO^+ (Cernicharo et al. 1989; Gammie et al. 1989). Many observational facts, such as the increase of radio continuum flux density, the existence of the high-velocity outflow, and the very compact core of ionized gas, etc., suggest that CRL 618 is now in a very active phase on the evolution from proto-planetary nebula to planetary nebula.

In order to examine the process of the transition to the planetary nebula, we have been mapping gas distribution by

[1] Nobeyama Radio Observatory, National Astronomical Observatory, Nobeyama, Minamimaki, Minamisaku, Nagano 384-13, Japan.
[2] Present address: Division of Earth Rotation, National Astronomical Observatory, Mizusawa, Iwate 023, Japan.
[3] Laboratory of Astronomy and Geophysics, Hitotsubashi University, Kunitachi, Tokyo 186, Japan.
[4] Mizusawa Astrogeodynamics Observatory, National Astronomical Observatory, Mizusawa, Iwate 023, Japan.
[5] Astronomical Institute, Tohoku University, Sendai, Miyagi 980, Japan.

various molecular lines in proto-planetary and planetary nebulae with the Nobeyama Millimeter Array (Shibata et al. 1989; Deguchi et al. 1992). In this paper, we present the results of aperture synthesis observations of ^{12}CO $J = 1$–0 in CRL 618. The distribution of the CO $J = 1$–0 line does not exhibit bipolar nor torus features but is rather spherically symmetric. We will discuss the structure of CO in the bipolar nebula.

The distance to CRL 618 is not well determined and we adopt the distance of 1.8 kpc according to Schmidt & Cohen (1981) throughout this paper.

2. OBSERVATIONS

We have observed CO $J = 1$–0 emission at 115.271 GHz from 1991 January to March using the Nobeyama Millimeter Array (NMA) at NRO.[6] The observations were made with three configurations of five 10 m antennas. We observed CRL 618 twice in each configuration and got a total of 28 independent baselines. We flagged out a part of obtained data because of bad quality for the weather condition and got the total on-source integration time of 28 hr. The maximum and the minimum projected baseline lengths were 110 kilowavelengths and 6.5 kilowavelengths, respectively. The derived synthesized beam was $3''.6 \times 3''.5$ (P.A. = 70°).

The antennas were equipped with SIS receivers, providing a system temperature (SSB) of about 600 K at 115 GHz. The backend was a 1024 channel digital FFT spectrocorrelator, called FX. We used an FX bandwidth of 320 MHz, which gave a total velocity coverage of 833 km s^{-1} and a velocity resolution of 0.81 km s^{-1}. The primary beam of the single antenna had a size of 1′ in diameter (HPBW) and was centered on the position of infrared source, R.A.(1950.0) = $04^h39^m33^s.8$, Decl.(1950.0) = +36°01′15″.0 (Westbrook et al. 1975).

The continuum source 3C 84 was used as an amplitude and phase calibrator. The adopted flux densities of 3C 84 were 8.0, 8.7, and 7.3 Jy in January, February, and March, respectively. The bandpass calibration was made from the observations of 3C 84 and 3C 273. Continuum data were taken by averaging visibility data of line-free channels. We used 400 channels which have velocities of over 170 km s^{-1} from line center as line-free channels in order to avoid the contamination of the high-velocity wing component (Gammie et al. 1989; Cernicharo et al. 1989). Line data were obtained by subtracting continuum components from the observed visibility. The line and continuum data were Fourier-transformed and CLEANed, respectively, by using the Astronomical Image Processing System (AIPS). We employed natural weighting to obtain maps. The rms noise level in the CO $J = 1$–0 velocity channel maps with 2.4 km s^{-1} resolution is 0.36 Jy beam^{-1}, and the rms noise in the continuum map with 320 MHz bandwidth is 30 mJy beam^{-1}.

3. RESULTS

3.1. CO $J = 1$–0 *Emission*

The integrated map of ^{12}CO $J = 1$–0 in a velocity range from $V_{LSR} = -44.5$ km s^{-1} to 8.3 km s^{-1} is presented in Figure 1. The convolved size of CO emission is about 15″ × 12″ at the 3 σ contour level. CO emission extends the northwest to southeast direction at the lower contours. However, it elongates to the east-west direction at the higher contours and forms an elliptical shape with the aspect ratio of 1.2 at the 11 σ contour level. These higher level contours extend to the south at the eastern part. These overall features are consistent with the CO ($J = 1$–0 and 2–1) and HC_3N maps observed by Bachiller et al. (1988) and Bujarrabal et al. (1988), with the beamsize of 22″, 11″, and 15″, respectively. The CO distribution shows strong central concentration. The emission peak position derived from two-dimensional Gaussian fitting to the area of higher flux density is R.A.(1950.0) = $4^h39^m34^s.01$, Decl.(1950.0) = +36°01′15″.9 and well coincident with 115 GHz continuum position (see later section; hereafter the peak position of continuum emission as the position center).

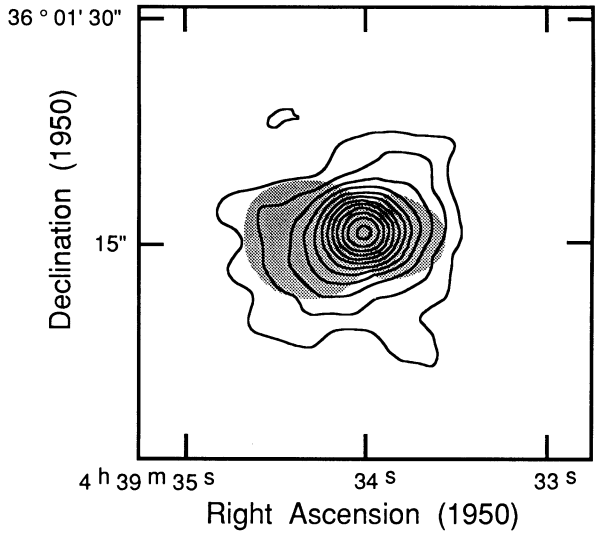

FIG. 1.—Integrated intensity map of the ^{12}CO $J = 1$–0 line for a velocity range from $V_{LSR} = -44.5$ to 8.3 km s^{-1} in CRL 618. The visible bipolar lobes are presented by a hatched region (adapted from Fig. 2 in Beckwith et al. 1984). Contour levels are in linear steps of 4.4 Jy beam^{-1} (2 σ level of map) starting from 3 σ level.

In Figure 2, we present velocity channel maps of CO $J = 1$–0 emission which were obtained by three-channel averaging corresponding to the velocity resolution of 2.4 km s^{-1}. These maps show that emission concentrates toward the position center and has only one peak except the two maps at the velocity of −25.8 and −23.4 km s^{-1}. Complex features changes from panel to panel. It seems that the systematic pattern, which should appear in the cases of spheroidal, ring or bipolar etc., can not be seen in these maps. We derived the position of the emission peak in each panel of Figure 2 using two-dimensional Gaussian fitting. The peak positions are scattered around the position center and coincident with that within 0″.8 in declination and 0″.9 in right ascension except the position at the velocity of −35.6 km s^{-1} which is apparently shifted to the east by 2″.3.

In the panel of $V_{LSR} = -20.9$ km s^{-1}, almost at the systemic velocity ($V_{LSR} = -21$ km s^{-1}), the contours elongate to the east-west direction and have the aspect ratio of 1.3 at the 5 σ contour level. A similar component elongated to the east-west direction can be seen in the panels of $V_{LSR} = -25.8$, −18.5, and −11.2 km s^{-1}. The very weak north-south elongation, which is perpendicular to the axis of visible bipolar lobes, can

[6] NRO (Nobeyama Radio Observatory) is a branch of the National Astronomical Observatory, an inter-university research institute operated by the Ministry of Education, Science, and Culture, Japan.

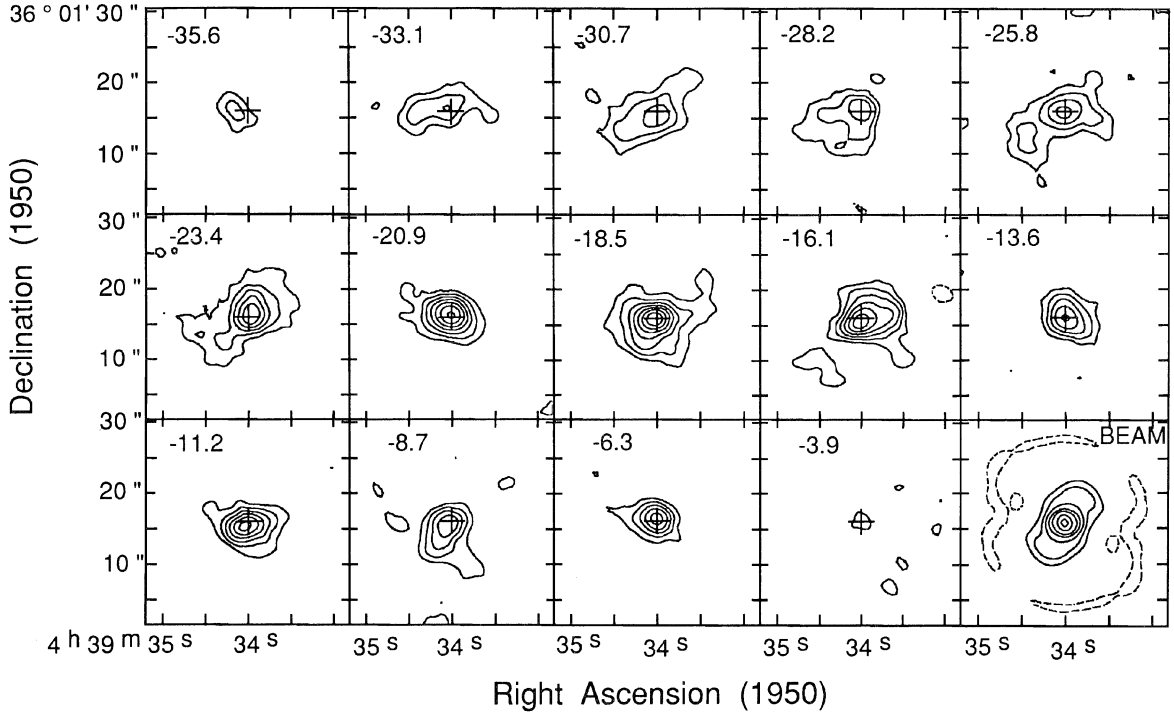

FIG. 2.—Velocity channel maps of the ^{12}CO $J = 1$–0 emission in CRL 618. Each map was obtained by three-channel averaging corresponding to a velocity resolution of 2.4 km s^{-1}. The panels are labeled with the LSR radial velocities. The position of the continuum peak is marked with the cross (+). Contour levels are in linear steps of 0.72 Jy beam^{-1} (2 σ level of the maps) from 3 σ level and broken contours are for negative intensities. The beam, which had a size of 3.″6 × 3.″5 (HPBW), is presented in the last panel, in which the contour levels are −10%, 10%, 30%, 50%, 70%, and 90% of the peak intensity.

be recognized in the panels of $V_{LSR} = -28.2$, -23.4, -13.6, and -8.7 km s^{-1}. A notable feature is a "horn"-like feature extended toward the southeast direction in the blueshifted velocity maps at the velocities from $V_{LSR} = -23.4$ to -30.7 km s^{-1}. The position angles of these horns are between 105° and 135°. Though this hornlike feature appears only at the first and the second levels of contours (3 and 5 σ levels, respectively) in Figure 2, the large extension (approximately 7″ × 10″) of this feature and the presence in several channel maps assure that it is real.

We show position-velocity diagrams at position angles of 0° and 90° through the position center in Figure 3*a* and 3*b*. These maps resemble each other in appearance. Two emission peaks are seen at the velocities of $V_{LSR} = -18$ and -11 km s^{-1}. The emission is concentrated to the position center. Several spurs extend from the position center at almost constant velocities. The contours around the blue peak ($V_{LSR} = -18$ km s^{-1}) are slightly tilted in Figure 3*b*, in which the emission contours shift to the north in the blue side of the peak and to the south in the red side of the peak. Figure 3*a* shows that a weak extension which has velocities between $V_{LSR} = -35$ and -20 km s^{-1} extends to the east. This extension is equivalent to the hornlike feature seen in Figure 2 toward the southeast direction in the blueshifted velocity maps lower than the systemic velocity ($V_{LSR} = -21$ km s^{-1}). And a red emission tail, which has velocity larger than $V_{LSR} = 0$ km s^{-1}, is seen at the position center.

Figure 4 shows the CO $J = 1$–0 line profile obtained by integrating all flux within a 22″ × 22″ square centered on the position center in the velocity channel maps. We fitted the parabolic formula,

$$I(V) = I_0\{1 - (V - V_c)^2/V_0^2\}\,; \quad |V - V_c| < V_0$$

(Knapp & Morris 1985), to the observed line profile and got the center velocity of $V_c = -20.5$ km s^{-1} and the expansion velocity of $V_0 = 20.6$ km s^{-1}. These values are consistent with single-dish results $V_c = -21.3$ km s^{-1} and $V_0 = 21.5$ km s^{-1} (Knapp & Morris 1985) considering our sampling interval of 2.4 km s^{-1}. The best fit is presented in Figure 4 with a dashed line. And residuals between observed profile and fitted parabola are also shown in Figure 4 by open circles and a thin line. The observed line profile can be approximately fitted by the parabolic shape, but two large dips at $V_{LSR} = -26$ and -14 km s^{-1} are notable in Figure 4. The residuals from the fitted curve at these dips (about 5 Jy) exceed 3 σ level of the noise which is deduced from the deviation of the residuals in the both sides of the line. The standard deviations of residual are 2.52 Jy in line area, from $V_{LSR} = -40$ km s^{-1} to 0 km s^{-1}, and 1.47 and 1.74 Jy in blue and red side out of the line, respectively. However, these dips may be caused by noise owing to relatively low S/N ratio and/or low velocity resolution of a 2.4 km s^{-1} of our line profile. If the dips of the observed line profile are real, not resulted from noise, it is suggested that CO gas in CRL 618 has a complex velocity component within a uniform spherical shell expanding with constant velocity. The single-dish CO (1–0) profile did not show such dips (e.g., Fig. 1*c* of Bachiller et al. 1988). One possibility, which can explain the discrepancy between the single dish profile and our interferometric profile, is a sensitivity of millimeter array. Present inter-

ferometric observations are not sensitive to the structure larger than about 30″. If CO emission is extended at $V_{LSR} = -27$ km s^{-1} and -13 km s^{-1}, the dip will appear around those velocities. Our integrated flux in the ^{12}CO line is 583 Jy km s^{-1} and is about 60% of that of the single-dish observation (Bachiller et al. 1988).

3.2. *High-Velocity Outflow*

In our observations, we have detected the red wing component of a high-velocity outflow but not the blue wing component. In Figure 4, the average flux density is positive (1.8 ± 0.4 Jy) in the velocity range of $V_{LSR} = 0$ to 25 km s^{-1}, while it is near zero at the lower velocities ($V_{LSR} = -45$ to -70 km s^{-1}). This emission appears as the emission tail concentrated on the center position in Figures 3*a* and 3*b*. We consider that this is the red wing component of a high-velocity outflow. To confirm the detection of the high-velocity component, we have made an integrated map for a velocity range from $V_{LSR} =$ 1.0 km s^{-1} to 32.7 km s^{-1}. This integrated map shows that the CO emission was detected over 7 σ levels and the deconvolved extension (FWHP) of this emission was 3″ in the east-west direction and ≤0.″5 in the north-south direction centered on 0.″5 south from the position center. This result supports the idea that the high-velocity outflows occur in very compact region centered on the ionized core. The blue wing component

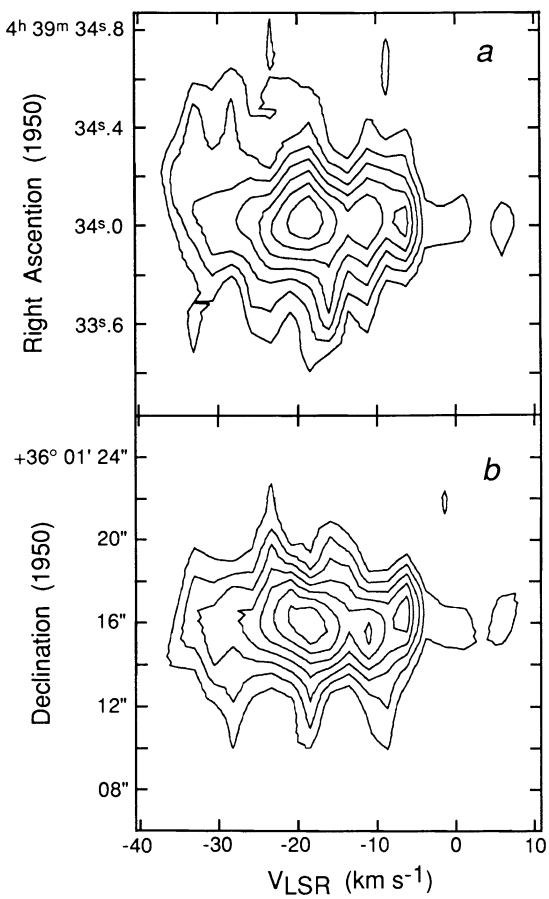

FIG. 3.—Position-velocity diagrams at position angles of (*a*) 90° and (*b*) 0° through the position of the continuum peak. Contour levels are in linear steps of 0.72 Jy beam^{-1} (2 σ level of the maps) from 3 σ level.

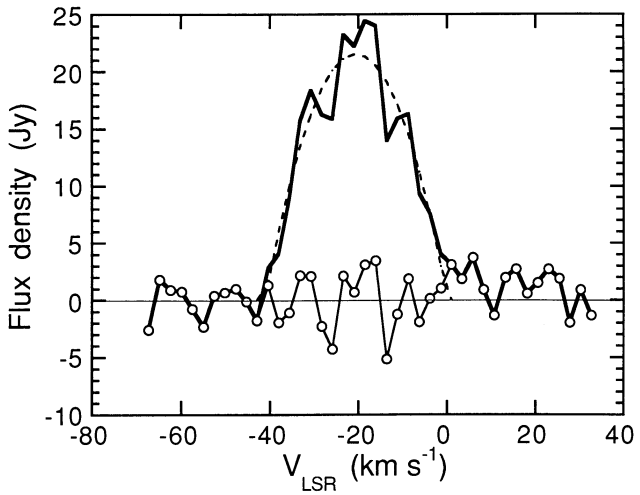

FIG. 4.—^{12}CO $J = 1$–0 line profile toward the position of the continuum peak. Thick solid line shows the integrated flux within the 22″ × 22″ square centered on the position of continuum peak. The parabola curve was fitted to the observed profile and result is shown by dashed line. Open circles and thin lines represent the residuals between the observed profile and the fitted parabola.

can not be seen in Figures 3 and 4. This is partly caused by the absorption of the continuum emission by the high-velocity outflow gas. In practice, the interferometric HCN observations (Neri et al. 1992) show a strong absorption feature in a velocity range from -60 to -40 km s^{-1}.

A very high-velocity molecular outflow was detected in the lines of CO, HCO^+, HCN, and HC_3N of CRL 618 with the terminal velocity of about 200 km s^{-1} (Cernicharo et al. 1989; Gammie et al. 1989). Neri et al. (1992) made aperture synthesis observations of HCN $J = 1$–0 line in CRL 618 using IRAM interferometer. They found that the red wing arises from a very small region (≤0.″5 × 0.″5) located 1″ west of the ionized core and the blue wing comes from a rather large area (2″ in the east-west direction and ≤0.″5 in the north-south direction) extending to the east of the ionized core. This result is consistent with the bipolar flow model of Carsenty & Solf (1982) in which the axis of bipolar lobes inclines about 45° with respect to the line of sight, the east lobe exists in near side and the west lobe in far side, and mass flows along this axis.

Interferometric high resolution observations with HCN $J = 1$–0 (Neri et al. 1992) and ^{12}CO $J = 1$–0 (this paper) in CRL 618 show that the high-velocity outflow arises from very compact region with a size of a few arcseconds or less and higher resolution observation is necessary to investigate the mechanisms of the high-velocity outflow. Intensity of the high-velocity wing in the CO $J = 1$–0 line is much weaker than those in $J = 2$–1 and 3–2 lines. The ratios of the high-velocity wing intensity to the peak intensity are 0.009, 0.06, and 0.14 in the CO $J = 1$–0, 2–1, and 3–2 line, respectively (Cernicharo et al. 1989; Gammie et al. 1989). Hence, high-resolution observations with the CO $J = 2$–1 and 3–2 lines are useful in order to investigate the high-velocity outflow in CRL 618.

3.3. *Continuum Emission*

We made a 115 GHz continuum map. The emission was well fitted by a two-dimensional Gaussian with a size of 3.″9 × 3.″5

(FWHP). Because the emission size is almost the same as that of synthesized beam, it is estimated that the continuum is emitted from a pointlike source of the size smaller than 1".5. The peak position is derived to be R.A.(1950.0) = $4^h39^m34^s.01$, Decl.(1950.0) = +36°01'16".0. This source size and position coincides with the results of more high-resolution observations by VLA at low frequencies (Kwok & Bignell 1984).

Total source flux density of continuum emission at 115 GHz is 1.48 Jy. Martín-Pintado et al. (1988) fitted the infrared energy distribution of CRL 618 by two blackbodies with temperatures of 95 and 280 K. From their results, the contribution of the dust emission to the total continuum flux density is estimated to be less than 0.01 Jy at 115 GHz. We may consider all of 1.48 Jy comes from a free-free emission of the ionized gas. Our result and that of VLA observations (6, 2, and 1.3 cm; Kwok & Bignell 1984) leads the spectral index (ν^α) is $\alpha = 1.4$. Martín-Pintado et al. (1988) observed continuum fluxes at the frequencies of 22, 88, 147, and 232 GHz and fitted a cylindrical isothermal ionized gas model with power-law density distribution in order to explain the radio spectra obtained from them and Kwok & Bignell (1984). Our value of the total flux density is consistent with the value estimated from their model calculations.

4. DISCUSSION

4.1. *Comparison with Other Objects*

Plenty of objects which have a bipolar structure in visible wavelength are known among the proto-planetary and planetary nebulae (e.g., Calvet & Cohen 1978). The bipolar structure reminds us of the existence of a dense toroidal disk which surrounds the central star and has the same axis as the bipolar lobes (Morris 1987). For example, CRL 2688, which is a typical bipolar proto–planetary nebula and resemble with CRL 618 very well but has no ionized gas, was suggested to have a toroidal disk which is located perpendicular to the visible lobes and associated with the dark lane (Nguyen-Q-Rieu, Winnberg, & Bujarrabal 1986; see also Nguyen-Q-Rieu & Bieging 1990, and references therein). Among the planetary nebulae, NGC 2346 is one of the well observed bipolar objects by CO molecular line. Bachiller et al. (1989b) showed that an expanding CO ring surrounds the central star and the waist of the bipolar ionized gas in NGC 2346. An optical [N II] line emission (Walsh 1983) is closely associated in both position and velocity with CO emission in NGC 2346 (Healy & Huggins 1988; Bachiller et al. 1989b). This fact suggests that CO gas constitutes the walls of the cavity in which the ionized gas is flowing.

There is an object which has not been known as a bipolar nebula until now but have the toroidal structure of molecular gas. IRAS 21282+5050 is a very compact, optically unresolved (smaller than 1".2) planetary nebula (Cohen & Jones 1987). Shibata et al. (1989) found that CO gas in IRAS 21282+5050 has a toroidal structure whose axis lies along the east-west direction and is normal to the line of sight.

In the case of CRL 618, the bipolar lobes and the infrared source at the midpoint of lobes suggest the existence of a toroidal disk. By the VLA observation of the ionized gas, Kwok & Bignell (1984) found that the major axis of the continuum emission increases the size with wavelengths although the minor axis has the same length of about 0".1 in each wavelength (1.3, 2, and 6 cm). They concluded that the ionization of CRL 618 is bounded in the north-south direction (along minor axis) but not in the east-west direction (major axis). That is, there is a density gradient in which the density of a neutral gas increasing toward the plane perpendicular to the axis of the bipolar lobes from the polar direction.

Present results by the ^{12}CO $J = 1$–0 line, however, show no clear evidence of the toroidal structure around CRL 618. Figure 1, the integrated CO map, shows a small elongation to the east-west direction. In Figure 2, CO map shows a peak concentrated toward the position center in each panel. It does not exhibit any intensity minimum near the position center and any elongation to the north-south direction. Similarly, HCN $J = 1$–0 observations using the IRAM interferometer (Neri et al. 1992) show no evidence for the toroidal structure. According to other observational results such as the bipolar lobes, the ionized core elongated toward the east-west direction, the distribution of H_2 emission and the kinematics from optical emission lines etc., it is thought that we can not deny the presence of a density contrast, i.e., a toroidal structure in the envelope of CRL 618. Hence, we make a hypothesis that the structure in the envelope can not be resolved because CRL 618 is so young that the CO structure has not developed enough. Considering the interacting stellar wind model for the formation of planetary nebula (e.g., Volk & Kwok 1985), a circumstellar envelope ejected from the AGB star is swept up by a fast wind ejected by the central star and is ionized by the UV radiation from the central star. Hence, neutral gas around planetary nebula closely contacts with the ionized gas at its inner side. The size of a ionized gas in CRL 618 is 0".7 × 0".1 at 6 cm continuum emission (Kwok & Bignell 1984). We noted, as previously mentioned, that the length of the major axis may be a little longer than 0".7 at longer wavelength but the length of the minor axis will be constantly 0".1. Hence the cavity, which exists in the neutral gas of CRL 618 and is filled with an ionized gas and a fast wind, is very small and cannot be resolved with the resolution of the present observations of about 3".5.

It is interesting to compare the size of CO structure, ring or spheroidal shell, between CRL 618 and other planetary nebulae. We present the sizes of CO structure and ionized gas of CRL 618, NGC 2346, NGC 6720, and NGC 7027 in Table 1. We estimated the linear CO sizes in NGC 2346, NGC 6720, and NGC 7027 from the maps obtained by single-dish observations (NGC 7027 was combined interferometric observations and single-dish ones). Our observation of CRL 618 is interferometric and contains the missing flux. Therefore the CO size estimated from the interferometric results is probably a lower limit for the size of CO distribution. Also, we must take into account a CO photodissociation by interstellar UV radiation. Mamon, Glassgold, & Huggins (1988) calculated CO photodissociation radii in circumstellar envelopes and predicted a photodissociation radius of 6.67×10^{17} cm (0.22 pc) for a mass-loss rate of $5 \times 10^{-5}\ M_\odot\ \mathrm{yr}^{-1}$ and an expansion velocity of 15 km s^{-1}. The similar value (0.26 pc) has been obtained by Yamamura et al. (1993). Though the photodissociation radius increases with the mass-loss rate, it is suitable to conclude that the outer radius of all nebulae in Table 1 are not suffered by the interstellar UV photodissociation. The mass-loss rate of NGC 6720 is unknown. However, from the existence of large molecular gas (0.1 $M_\odot$; Bachiller et al. 1989a), it is considered that NGC 6720 had a similar mass loss rate with the other three nebulae. CO size of CRL 618 is smaller than other planetary nebulae. If we assumed the typical size of the outer radius of a ring structure in CO gas around evolved planetary nebula as 0.13 pc, and if CO gas in CRL 618 expand with a constant velocity of 20 km s^{-1}, it takes about

TABLE 1

THE SIZES OF THE CO STRUCTURE AND THE IONIZED GAS IN PLANETARY NEBULAE

Parameter	CRL 618	NGC 2346	NGC 6720	NGC 7027
Type of the structure	Spherical	Ring	Ring	Spheroidal shell
Outer radius of the structure (pc)	0.05[a]	0.16[b]	0.09[b]	0.15[c]
Inner radius of the structure (pc)	...	0.05	0.03	0.02
The size of ionized gas (pc)	0.006 × 0.001	0.35 × 0.25	0.21 × 0.16	0.052 × 0.035
Distance (kpc)	1.8	1.0	0.5	0.9
Mass-loss rate ($M_\odot$ yr^{-1})	10^{-4}	$>5 \times 10^{-5}$	...	3×10^{-4}
References	1, 2	3, 4	5	6, 7

NOTES.—References: Schmidt & Cohen 1981; Bachiller et al. 1988; Bachiller et al. 1989b; Gathier et al. 1986; Bachiller et al. 1989a; Bieging et al. 1991; Masson 1989.

[a] Estimated from interferometric results (this paper).

[b] Estimated from single dish results.

[c] Estimated from the results which obtained from the data combined interferometric and single-dish observations.

4000 yr until the outer radius of CRL 618 reaches to 0.13 pc from 0.05 pc. This is a reasonable time scale for the formation of planetary nebula. Above estimations are very rough because the uncertainty in the distance is large except the case of NGC 7027 (Masson 1989). However, the differences in the size of ionized gas are very clear even if the uncertainty in the distances exists. The size of ionized gas in CRL 618 is smaller by 1/30 or less than those in other nebulae.

4.2. CO *Structure of CRL 618*

The ^{12}CO $J = 1$–0 maps, in which any systematic features of axisymmetric structure cannot be seen, suggest that the approximate structure of CO gas in CRL 618 may be spherical and this spherical structure contains some distinctive feature which will be mentioned below. We will note first about spheroidal features seen in some maps. In our integrated CO map, Figure 1, higher contours show the elliptical shape which weakly elongates to the east-west direction. Same weakly elongated features are present in the channel-velocity maps, Figure 2, at the $V_{LSR} = -20.9$, -18.5, and -11.2 km s^{-1}. This may suggest the presence of a spheroidal structure in CO gas. If this spheroid has the same axis with the bipolar lobes, i.e., inclined by about 45° with respect to the line of sight and has an expanding motion, the centroid of CO emission will change its position on the channel maps systematically with velocity. The systematic change, however, cannot be recognized in Figure 2. This means that the axis of the spheroid lies perpendicular to the line of sight and differs from the axis of bipolar lobes, that is, CO gas has a different distribution from the visible bipolar lobes. Another idea to explain the elongated spheroidal feature is a presence of the expanding oblate spheroid whose axis is perpendicular to the line of sight and lies along the north-south direction. This oblate spheroid needs not the systematic change in the velocity-channel maps and can contain the bipolar lobes within itself. In both cases, the axis of CO gas is different from that of bipolar lobes and it means the axis of mass loss is different between the past and the present. Because the CO $J = 1$–0 line is optically thick in the envelope (Bachiller et al. 1988), the CO contour is not a tracer of the density profile but rather a tracer of a kinetic temperature distribution. Therefore, the elongation of the spheroid in the east-west direction may be caused by the kinetic temperature gradient which is slightly higher along the bipolar axis. It is possible that the material along the bipolar axis is heated up more by the preferential escape of optical or infrared photons along this axis. The highest level contour in Figure 2 ($V_{LSR} = -18.5$ km s^{-1}) corresponds to the temperture of 36 K [the conversion of the flux density per beam to the brightness temperature is 7.3 K/(Jy beam^{-1})].

The next distinct feature is the "horn" extended toward the southeast in the blueshifted velocity in Figure 2. This horn also appears in Figure 3*a*. It is considered that the horn reveals a part of CO gas which is affected by a blue component of the bipolar flow. Optical observations suggest that the eastern visible lobes exist in near side than the western lobe and the optical lines are blueshifted in the eastern lobe and redshifted in the western lobe (Carsenty & Solf 1982). The horn coincides with these optical observations and suggest that the CO gas in CRL 618 may show a weak sign of an interaction with bipolar flow. We cannot find a feature which corresponds to the red component of bipolar flow. Bachiller et al. (1988) present a position-velocity diagram at the position angle of 90° through the continuum center for ^{12}CO $J = 2$–1 emission in their Figure 2. In that diagram, they found an asymmetrical trend in which the lines are blueshifted in eastern positions and redshifted in western position. Our Figure 3*a* reveals a similar trend to that diagram.

Cernicharo et al. (1989) made strip maps with the ^{12}CO $J = 2$–1 line using the IRAM 30 m telescope and reported that two emission peaks separated by 4″–6″ at $V_{LSR} = -17$ and -25 km s^{-1}, respectively, are found in the east-west strip map through the continuum center. This clear bipolarity cannot be seen in any of our ^{12}CO $J = 1$–0 results, ^{12}CO $J = 2$–1 results by Bachiller et al. (1988) and HCN $J = 1$–0 results by Neri et al. (1992). Although the discrepancy may be caused by the difference in a grid spacing in the observations, Bachiller et al. observed with about 6″.5 gridding, or by the differences in the transition and molecular species, it is necessary to make a higher resolution observation with ^{12}CO $J = 2$–1 emission.

Finally, we consider the model of CO structure in CRL 618. Our ^{12}CO $J = 1$–0 results do not show the toroidal nor bipolar structure but concentrated on the center having some weak spurs. However, the optical, H_2, and VLA observations (Westbrook et al. 1975; Carsenty & Solf 1982; Beckwith et al. 1984; Burton & Geballe 1986; Kwok & Bignell 1984) suggested the existence of the toroidal structure. Hence, we conclude that a dense toroidal disk, which surrounds the central star, collimates the high-velocity outflows and produces the bipolar features, is embedded in a rather uniform spherically symmetric CO gas. And it is considered that we could not observe this dense toroidal disk owing to the compactness of the disk or obscuring by the thick spherical CO gas which

surrounds the disk. This model can be adapted to the case of CRL 2688, in which ^{12}CO $J = 1–0$ shows spherical feature (Kawabe et al. 1987; Truong-Bach et al. 1990) but some other molecular lines show disk feature near the central part (see Nguyen-Q-Rieu & Bieging 1990, and references therein). And this model suggests that the mass loss ejected the matter isotropic in the early stage of proto-planetary nebula evolution and changes to the nonisotropic ejection which makes the toroidal structure in the latter stage. To construct more accurate model, the higher spatial and higher velocity resolution observations or the comparison with model calculation are necessary. We will try to make a more quantitative model by comparing our observation with model calculations in future work.

We would like to thank the staff of NMA for the operation of the interferometer in our observation and the support in the data reduction. K. M. S. thanks the Japan Society for the Promotion of Science for financial support.

REFERENCES

Bachiller, R., Bujarrabal, V., Martín-Pintado, J., & Gómez-González, J. 1989a, A&A, 218, 252
Bachiller, R., Gómez-González, J., Bujarrabal, V., & Martín-Pintado, J. 1988, A&A, 196, L5
Bachiller, R., Planesas, P., Martín-Pintado, J., Bujarrabal, V., & Tafalla, M. 1989b, A&A, 210, 366
Beckwith, S., Beck, S. C., & Gatley, I. 1984, ApJ, 280, 648
Bieging, J. H., Wilner, D., & Thronson, H. A. 1991, ApJ, 379, 271
Bujarrabal, V., Gómez-González, J., Bachiller, R., & Martín-Pintado, J. 1988, A&A, 204, 242
Burton, M. G., & Geballe, T. R. 1986, MNRAS, 223, 13P
Calvet, N., & Cohen, M. 1978, MNRAS, 182, 687
Carsenty, U., & Solf, J. 1982, A&A, 106, 307
Cernicharo, J., Guélin, M., Martín-Pintado, J., Peñalver, J., & Mauersberger, R. 1989, A&A, 222, L1
Cohen, M., & Jones, B. F. 1987, ApJ, 321, L151
Deguchi, S., Claussen, M. J., & Goldsmith, P. F. 1986, ApJ, 303, 810
Deguchi, S., Izumiura, H., Nguyen-Q-Rieu, Shibata, K. M., Ukita, N., & Yamamura, I. 1992, ApJ, 392, 597
Gammie, C. F., Knapp, G. R., Young, K., Phillips, T. G., & Falgarone, E. 1989, ApJ, 345, L87
Gathier, R., Pottasch, S. R., & Pel, J. W. 1986, A&A, 157, 171
Healy, A. P., & Huggins, P. J. 1988, AJ, 95, 866
Kawabe, R., et al. 1987, ApJ, 314, 322
Knapp, G. R., & Morris, M. 1985, ApJ, 292, 640
Kwok, S., & Bignell, R. C. 1984, ApJ, 276, 544
Kwok, S., & Feldman, P. A. 1981, ApJ, 247, L67
Mamon, G. A., Glassgold, A. E., & Huggins, P. J. 1988, ApJ, 328, 797
Martín-Pintado, J., Bujarrabal, V., Bachiller, R., Gómez-González, J., & Planesas, P. 1988, A&A, 197, L15
Masson, C. R. 1989, ApJ, 336, 294
Morris, M. 1987, PASP, 99, 1115
Neri, R., García-Burillo, S., Guélin, M., Cernicharo, J., Guilloteau, S., & Lucas, R. 1992, A&A, 262, 544
Nguyen-Q-Rieu, & Bieging, J. H. 1990, ApJ, 359, 131
Nguyen-Q-Rieu, Winnberg, A., & Bujarrabal, V. 1986, A&A, 165, 204
Schmidt, G. D., & Cohen, M. 1981, ApJ, 246, 444
Shibata, K. M., Tamura, S., Deguchi, S., Hirano, N., Kameya, O., & Kasuga, T. 1989, ApJ, 345, L55
Thronson, H. A. 1981, ApJ, 248, 984
Truong-Bach, Morris, D., Nguyen-Q-Rieu, & Deguchi, S. 1990, A&A, 230, 431
Volk, K., & Kwok, S. 1985, A&A, 153, 79
Walsh, J. R. 1983, MNRAS, 202, 303
Westbrook, W. E., Becklin, E. E., Merrill, K. M., Neugebauer, G., Schmidt, M., Willner, S. P., & Wynn-Williams, C. G. 1975, ApJ, 202, 407
Wynn-Williams, C. G. 1977, MNRAS, 181, 61P
Yamamura, I., Onaka, T., Kamijo, F., Izumiura, H., & Deguchi, S. 1993, PASJ, in press